Tail-Oxidized Cholesterol Enhances Membrane Permeability for Small Solutes

Agnieszka Olżyńska[1,*,§], Waldemar Kulig[2,*,§], Heikki Mikkolainen[3], Tomasz Czerniak[4,#], Piotr Jurkiewicz[1], Lukasz Cwiklik[1], Tomasz Rog[2], Martin Hof[1], Pavel Jungwirth[5], Ilpo Vattulainen[2,3,6]

[1] J. Heyrovský Institute of Physical Chemistry, Czech Academy of Sciences, Dolejškova 3, 18223 Prague 8, Czech Republic

[2] Department of Physics, University of Helsinki, P. O. Box 64, FI-00014 Helsinki, Finland

[3] Computational Physics Laboratory, Tampere University, P. O. Box 692, FI-33014 Tampere, Finland

[4] Faculty of Biotechnology, University of Wrocław, Joliot-Curie 14A, 50-383 Wrocław, Poland

[5] Institute of Organic Chemistry and Biochemistry, Czech Academy of Sciences, Flemingovo nám. 2, 16610 Prague 6, Czech Republic

[6] MEMPHYS-Center for Biomembrane Physics

[*] These authors contributed equally to this work.

[#] Present address: Laboratory of Synthetic Membrane Biology, Technical University Dresden, Arnoldstrasse 18, 01307 Dresden, Germany

[§] Corresponding author(s): agnieszka.olzynska@jh-inst.cas.cz (A.O.) and waldemar.kulig@helsinki.fi (W.K.)

Abstract

Cholesterol seals human cellular membranes against water and water-soluble solutes by filling the voids between phospholipid molecules. Also, its presence modulates function of membranes as semipermeable barriers. It is known that even small modifications in the chemical structure of cholesterol can lead to strong alteration of membrane properties. In this work, we apply fluorescence methods as well as molecular dynamics simulations to characterize changes in lipid membrane permeability induced by cholesterol oxidation. The studied 7β-hydroxycholesterol (7β-OH-chol) and 27-hydroxycholesterol (27-OH-chol) represent two distinct groups of oxysterols, namely, ring- and tail-oxidized cholesterols, respectively. Our previous research showed that oxidation of cholesterol tail only marginally affects the structure of lipid bilayer. On the other hand, it disturbs membrane dynamics introducing new rapid type of trans-bilayer movement of the sterol – bobbing. Herein we show that bobbing of 27-OH-chol accelerates fluorescence quenching of NBD-lipid in the inner leaflet of liposomes by dithionite added to the liposomal suspension. Systematic experiments using fluorescence quenching spectroscopy and microscopy led to conclusion that the presence of 27-OH-chol increases membrane permeability to dithionite anion. Atom-scale molecular dynamics simulations demonstrate that this oxysterol also facilitates water transport across the membrane. All these findings support the view that oxysterol bobbing introduces sequential disturbance in the hydrophobic core of the membrane and is capable of aiding water molecules, as well as small water-soluble molecules, across lipid bilayer. This permeabilization can have many important consequences for eukaryotic organisms. The effects described for 27-OH-chol were not observed for 7β-OH-chol – the ring-oxidized sterol.

Keywords: phospholipid bilayer, cholesterol, oxidative stress, oxysterol, liposomes, GUV, lipid flip-flop, membrane permeability, fluorescence quenching, molecular dynamics simulation

1. INTRODUCTION

Permeation of small molecules across cell membranes is of crucial importance to life. One of the underlying molecular mechanisms used by cells to control permeation through membranes is the level of cholesterol. Early studies documented that cholesterol decreases the permeability of water through model lipid membranes [1]. Subsequent investigations described this effect in detail [2-5], showing that the effect of cholesterol in lipid membrane structures is exceptionally prominent at the level of the cholesterol ring [3, 6]. Unbiased molecular dynamics (MD) simulations showed that the rate of spontaneous water translocation through a membrane decreases by a factor of seven when the content of cholesterol is increased from zero to 33 mol% [7]. This is in agreement with experimental studies that reported a four-fold reduction of water permeability through a bilayer containing 25 mol% of cholesterol compared to a pure phospholipid bilayer [1, 8-10]. Cholesterol has also been shown to decrease the membrane permeability to ions [11], small neutral molecules like glucose [12-13], and gases such as oxygen [14-15]. Recent MD simulation studies have further shown that the free energy barrier of translocating certain drugs and nanoparticles across a lipid bilayer increases with increasing cholesterol content [16-18]. In biological membranes, reduction of cholesterol concentration was observed to render them more permeable [9, 19].

Cholesterol thus plays a profound role in regulating the permeability of membranes. At the same time, cholesterol is a key molecule regulating a variety of other properties of animal cell membranes. For instance, cholesterol modulates the conformational ordering, thickness, and elastic properties of cell membranes, and it also strongly influences the phase and the dynamics of lipid membranes [20-21].

Although permeation mechanisms of chemically distinct molecules through lipid membranes are not identical (for a review on the topic, see Ref. [5, 22]), many properties of lipid bilayers correlate with their permeability. For example, for single-component lipid bilayers it has been shown that the average surface area per lipid and permeability are proportional to each other [2]. Membrane thickness has been demonstrated to significantly influence its permeability to protons and potassium ions, however, permeability to water and glycerol was only weakly affected [23]. Since cholesterol is known to both decrease the average surface area per lipid and increase membrane thickness, cholesterol-induced reduction of membrane permeability is to be expected. It was also demonstrated in a previous study that the permeability of a lipid membrane correlates with its surface density – the parameter that depends on both surface area and membrane thickness [24].

Permeability of biological membranes correlates with cholesterol distribution in cellular compartments and body organs. Among all cellular membranes, the highest cholesterol concentration is observed in the plasma membrane, which isolates cell interior from the outside environment [25]. Stratum corneum, *i.e.*, the external layer of skin, is also characterized by high cholesterol concentration [26] and known to be highly impermeable [27]. An organ with the highest cholesterol content is the brain, particularly the myelin sheets insulating the axons [28]. There are also various cholesterol-rich biomaterial applications mimicking nature, such as liposomes used in drug delivery, where high cholesterol content prevents leakage of encapsulated drugs [29-31]. This is a common strategy in currently approved therapies based on liposomes as drug carriers [32-33].

Of the ~80 sterols known in nature, only a few, including cholesterol, ergosterol, and some phytosterols, are crucial components of cellular membranes. Most of the remaining sterols are metabolites or signaling molecules. As a prime example, there is a large variety of different oxysterols that play important roles in biological processes such as apoptosis, lipid metabolism, and cholesterol homeostasis. Oxysterols can be formed by enzymatic cholesterol oxidation or by non-enzymatic autoxidation processes as a result of (mainly) oxidative stress involving reactive oxygen species (ROS) [34]. Oxysterols formed as products of enzymatic reactions have an additional polar group that is predominantly found in the sterol tail. These oxysterols often act as signaling molecules. In contrast, oxysterols that result from the exposure of cholesterol to ROS have additional polar groups attached to the steroid ring.

Although the effects of oxysterols on lipid bilayer properties have been extensively characterized (for a review see, *e.g.*, [35]), little is known about the ability of oxysterols to modulate membrane permeability. To the best of our knowledge, the only exception is 25-hydroxycholesterol (25-OH-chol), which was shown to increase membrane permeability to calcium and glucose [36-37]. At the same time, if this matter is considered from a more general point of view, oxidation of phospholipids is known to have severe detrimental effects on membrane permeability. For instance, the oxidation of polyunsaturated lipids can destabilize lipid membranes, leading to the formation of pores and the subsequent breakdown of the membrane [38].

Oxidation of cholesterol is known to alter its ability to modulate membrane properties [39]. This is somewhat surprising given that the structural differences between oxysterols and cholesterol are rather small (typically, one or two additional oxygen-containing polar groups). Moreover, the position of the additional oxygen-containing group is of great importance[39].

Motivated by this finding, we use here atomic-scale simulations and free energy calculations in conjunction with complementary experimental fluorescence techniques to elucidate how the presence of tail- and ring-oxidized sterols influences membrane permeability and related translocation processes such as lipid flip-flop. Molecular simulations have demonstrated their ability to unravel nanoscale properties of biological membranes [40]. As representatives of ring- and tail-oxidized sterols, we chose 7β-hydroxycholesterol (7β-OH-chol) and 27-hydroxycholesterol (27-OH-chol), respectively. We show in this work that they affect membrane permeability in very different ways.

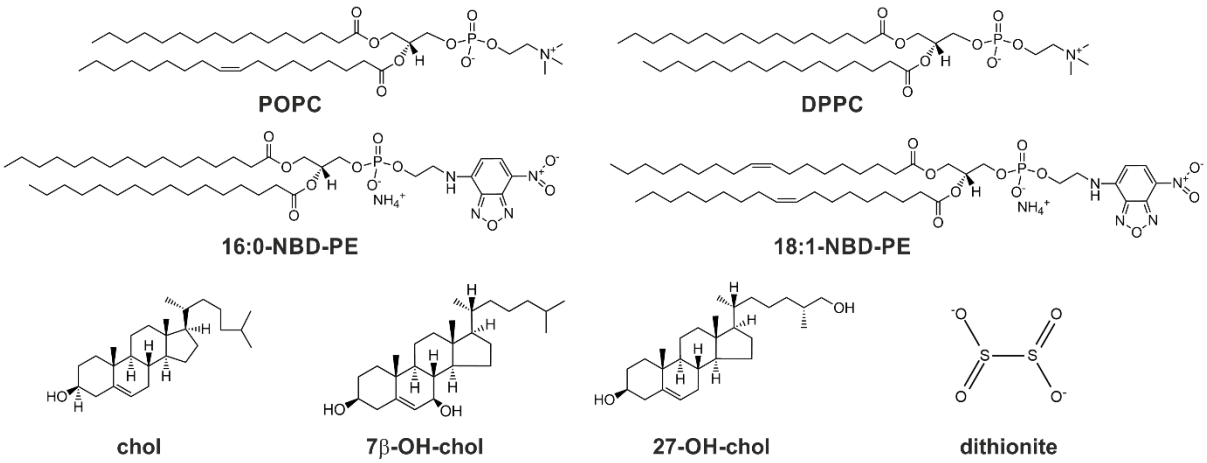

Figure 1. Chemical structures of compounds used in this study. POPC (1-palmitoyl-2-oleoyl-*sn*-glycero-3-phosphatidylcholine); DPPC (1,2-dipalmitoyl-*sn*-glycero-3-phosphatidylcholine); 16:0-NBD-PE (1,2-dipalmitoyl-*sn*-glycero-3-phosphatidylethanolamine-N-(7-nitro-2-1,3-benzoxadiazol-4-yl)); 18:1-NBD-PE (1,2-dioleoyl-*sn*-glycero-3-phosphatidylethanolamine-N-(7-nitro-2-1,3-benzoxadiazol-4-yl)); chol (cholesterol); 7β-OH-chol (7β-hydroxycholesterol); 27-OH-chol (27-hydroxycholesterol); and dithionite.

2. MATERIALS AND METHODS

Materials

Figure 1 depicts the compounds used in this work. 1-palmitoyl-2-oleoyl-*sn*-glycero-3-phosphatidylcholine (POPC), 1,2-dipalmitoyl-*sn*-glycero-3-phosphatidylcholine (DPPC), cholesterol (ovine wool) (chol), 7β-hydroxycholesterol (7β-OH-chol), 27-hydroxycholesterol (27-OH-chol), 1,2-dipalmitoyl-*sn*-glycero-3-phosphatidylethanolamine-N-(7-nitro-2-1,3-benzoxadiazol-4-yl) (16:0-NBD-PE), 1,2-dioleoyl-*sn*-glycero-3-phosphatidylethanolamine-N-(7-nitro-2-1,3-benzoxadiazol-4-yl) (18:1-NBD-PE), and 1,2-dioleoyl-*sn*-glycero-3-phosphatidylethanolamine-N-(cap biotinyl) (biotinylated DOPE) were obtained from Avanti Polar Lipids, Inc. (Alabaster, AL, USA). 4-(2-hydroxyethyl)piperazine-1-ethanesulfonic acid (HEPES), sodium chloride, ethylenedinitrilotetraacetic acid (EDTA), tris(hydroxymethyl)

aminomethane (Tris), and sodium dithionite were ordered from Sigma-Aldrich (St. Louis, MO, USA). Buffers were prepared using Mili-Q water (Milipore, USA). Merck (Darmstadt, Germany) supplied organic solvents of spectroscopic grade. All chemicals were used without further purification.

Preparation of LUVs

Extruded large unilamellar vesicles (LUVs) were prepared as described below. The required volumes of chloroform solutions of POPC and either cholesterol or one of the oxysterols were mixed with a fluorescent probe in a glass tube. The final molar ratio of lipid-to-probe was 200:1. Solvents were evaporated under a stream of nitrogen and the lipid film was kept under vacuum for at least 2 hours. Then, the dry lipid film was suspended in a 10 mM HEPES buffer (150 mM NaCl, pH 7.0, 0.2 mM EDTA). After 5 minutes of continuous vortexing the suspension of multilamellar vesicles was extruded through polycarbonate membranes with a nominal pore diameter of 100 nm (Avestin, Ottawa, Canada). The final total concentration of lipids including sterols was 20 μM.

Preparation of GUVs

Giant unilamellar vesicles (GUVs) were prepared using electroformation method developed by Angelova *et al*. [41], and modified later as described in Ref. [42]. Proper volumes of a chloroform solution of POPC, cholesterol/oxysterol (10 mol%), 18:1-NBD-PE (0.5 mol%), and biotinylated DOPE (2 mol%) were mixed in a glass tube to get 100 nmol of lipids per sample. 100 μL of these mixtures were spread with a Hamilton syringe on a pair of titanium plates and heated to approximately 40 °C to accelerate solvent evaporation. Lipid-coated plates were kept in vacuum for at least 1.5 h. Each pair of the titanium plates was connected using parafilm (Bemis, Neenah, WI, USA), which also serves as an isolator. The chamber formed this way was filled with ~900 μL of sucrose solution (285 mOsm) and sealed with parafilm. GUVs were formed by applying a sinusoidal alternating electrical current to the plates. The following sequence of voltages and frequencies were used: starting with a peak-to-peak voltage U = 0.15 V, the voltage was increased stepwise to 1.1 V at 10 Hz for 47.5 min, continuing with U = 1.1 V at 10 Hz for further 100 min, and finishing with U = 1.3 V at 4 Hz for 30 min.

NBD-Dithionite Quenching – Kinetics Measurements

Steady-state (SS) fluorescence measurements were performed on a Fluorolog-3 spectrofluorometer (model FL3-11; Jobin Yvon Inc., Edison, NJ) equipped with a Xenon-arc

lamp. NBD probe excitation and emission wavelengths were set at 470/544 nm. All fluorescence quenching kinetics were recorded using 1 and 7 nm excitation and emission slits, respectively.

The prepared samples were transferred to a 1 cm quartz cuvette and equilibrated at 37 ± 0.2 °C, unless specified otherwise, using water-circulating thermostat for 15 min before each measurement. Sodium dithionite powder was dissolved in a 100 mM TRIS buffer (pH 10.0) to get a 1 M solution. Fresh dithionite solution was added with a pipette to 1.5 mL LUV dispersion in the cuvette at time t_0 (140 seconds after starting the measurement when the stability of the fluorescence signal was confirmed) and briefly but vigorously mixed with a pipette. Fluorescence intensity $F(t)$ was continuously recorded until the time $t = t_1$ at which a Triton-100 solution was added to the cuvette. Average speed of fluorescence quenching within the interval (t_0, t_1) was calculated as:

$$\Delta Q = \frac{\int_{t_0}^{t_1}\left(1-\frac{F(t)}{F(t_0)}\right)dt}{\frac{1}{2}(t_1-t_0)^2} \quad . \tag{1}$$

The final concentration of dithionite in the sample was 50 mM.

NBD-Dithionite Quenching – Fluorescence Microscopy

Fluorescence microscopy measurements were performed using an Olympus FluoView 1000 confocal laser scanning microscope (Olympus, Hamburg, Germany) equipped with a UPlanSApo 60× water immersion lens with a numerical aperture of 1.2. An NBD dye was excited using a 488 nm continuous wave Sapphire laser (Coherent, Santa Clara, CA, USA) with an excitation intensity of 2-3 μW focused in a diffraction-limited confocal volume and detected with a PMT detector through a band-pass 490-525 nm filter.

The bottom surface of the observation chamber (Lab-Tek, NUNC, Germany) was prepared with the following steps. First, it was treated with biotin-conjugated bovine serum albumin (0.1 mg/mL) for ~30 min and washed carefully several times with MiliQ water afterwards. Later, streptavidin (20 μg/mL) was added to the chamber and left for incubation for ~15 min, followed by several washings with Mili-Q water. Next, 40 μL of the GUV sucrose solution (285 mOsm) was added to the observation chamber filled with 360 μL of 10 mM HEPES buffer (pH 7.4, 10 mM NaCl, 285 mOsm - fixed with glucose solution). GUVs were left to settle and create bindings between biotinylated DOPE and streptavidin for at least 30 min, and 10 μL of 1 M dithionite solution (solvent: 100 mM TRIS buffer, pH 10.0) was gently added to the chamber. Final dithionite concentration in the chamber was 25 mM. To study fluorescence quenching of

the probe in the GUV membrane, images of the area of interest were taken every 4 s for up to 25 min.

Atom-Scale Molecular Dynamics Simulations

We carried out all-atom molecular dynamics (MD) simulations of lipid bilayers containing 90 mol% POPC and 10 mol% cholesterol, 7β-OH-chol, or 27-OH-chol (denoted below as POPC/chol, POPC/7β-OH-chol, and POPC/27-OH-chol, respectively). Additionally, we studied a pure POPC bilayer (called POPC) as a control case. Detailed compositions of all bilayers are listed in Table 1. The initial structure of the POPC bilayer was created by arranging POPC molecules on an 8×8 grid, resulting in a bilayer consisting of two leaflets of 64 lipids each. Bilayers containing 10 mol% of a sterol were created by randomly replacing 14 lipid molecules with sterol molecules.

Table 1. Detailed compositions of all lipid bilayers explored in this work. Given here are the numbers of each molecule/ion type in the listed systems.

System	POPC	chol	7β-OH-chol	27-OH-chol	Na^+	Cl^-	Water
POPC	128				17	17	6366
POPC/chol	114	14			17	17	6366
POPC/7β-OH-chol	114		14		17	17	6366
POPC/27-OH-chol	114			14	17	17	6366

The all-atom OPLS force field [43-44] was used to describe the interactions, unless mentioned otherwise. The topologies of sterols were created as described in Ref. [39], while the parameters describing POPC molecules were taken from [45-46]. In order to restrain covalent bonds, the LINCS algorithm was used [47], allowing the use of a 2 fs time step. Analogously, the SETTLE algorithm was employed for water molecules [48]. Periodic boundary conditions were applied in all three directions. Long-range electrostatic interactions were computed using the particle mesh Ewald (PME) algorithm with a cutoff of 1.0 nm [49], Fourier spacing of 0.1 nm, and a sixth order interpolation of the mesh. A long-range dispersion correction to energy and pressure was added.

The Nosé-Hoover thermostat with a coupling constant of 0.4 ps was used to keep the system temperature at 310 K [50-51]. The bilayer and the solvent were coupled to separate thermostats. The Parrinello-Rahman barostat was employed to keep pressure at 1 atm with a coupling

constant of 1 ps and a compressibility of 4.5×10^{-5} bar^{-1} [52]. A semi-isotropic scheme of pressure coupling was used, meaning that the pressure in the *x* and *y* directions (*i.e.*, the bilayer plane) was coupled separately from the pressure in the *z* direction (*i.e.*, bilayer normal). The GROMACS 4.6.x software package was used in all simulations [53-54]. As to equilibration, each system was first energy-minimized using the steepest descent algorithm, and then equilibrated in the NpT ensemble for at least 50 ns.

For free energy analysis, two series of umbrella sampling simulations were performed. In the first series, a single water molecule was pulled from the membrane-water interface to the center of a bilayer (POPC, POPC/chol, POPC/7β-OH-chol, or POPC/27-OH-chol), and in the second series a single POPC molecule was pulled from one leaflet of the lipid bilayer to the other. Umbrella sampling was performed with a total of 32 (first series) or 71 (second series) windows. The initial configurations for umbrella windows were selected randomly at 0.1 nm intervals. Each window was simulated for 50 or 100 ns (first or second series, respectively), where the first 20 or 40 ns (first or second series, in respective order) were used for equilibration. In each umbrella window, the pulled molecules were restrained using a harmonic potential with a force constant of 3000 kJ mol^{-1} nm^{-2}. The restrains were applied only along the reaction coordinate (*i.e.*, the normal to the bilayer surface) while the pulled molecules were free to move in other directions.

For completeness, let us mention that additional pulling simulations were performed prior to actual umbrella sampling simulations to generate a series of configurations for umbrella sampling. In the pulling simulations, the investigated molecules were pulled along the *z*-axis, and the center of mass (COM) of a water molecule or the COM of the phosphate group of POPC molecule was used as the pulling group. The force constant applied to the pulled water molecule was 1000 kJ mol^{-1} nm^{-2} and the pull rate was 0.002 nm ns^{-1}. The force constant applied to the pulled phosphate group (when pulling POPC) was 500 kJ mol^{-1} nm^{-2} and the pull rate was 0.002 nm ns^{-1}.

The weighted histogram analysis method (WHAM) was used to compute the potential of mean force (PMF) along the reaction coordinate. WHAM analysis was performed using the GROMACS *g_wham* tool with 284 bins (when pulling POPC) or 128 bins (when pulling water) and a 0.025 nm bin width. Statistical uncertainties were estimated using bootstrap analysis. A bootstrap sample size of 100 was used in this study.

3. RESULTS

Tail-Oxidized Sterol Modulates Membrane Permeability and/or Lipid Flip-Flop

Fluorescence quenching experiments were performed on oxysterol-containing POPC LUVs at 37 °C. An NBD fluorescent lipid analog incorporated in the lipid bilayer of the LUVs was irreversibly quenched by dithionite added to the liposomal dispersion. The kinetics of the quenching process was documented by measuring fluorescence intensity in time after the dithionite addition. The obtained results, normalized to 1 for the signal before the quencher addition and to 0 for the completed quenching, are shown in Figure 2. The measurements were performed separately for two different NBD lipids.

Immediately after the quencher addition (in 140 s after starting the measurement), fluorescence intensity drops to about half of its initial value. This results from the dithionite molecules accessing the readily available outer lipid layer of the LUV membrane, where it quenches all molecules of NBD lipid. At this short time scale (a few seconds), the molecules of NBD lipid-analogs located in the inner lipid layer are unaffected and still fluoresce. The initial drop of fluorescence intensity is followed by slower quenching kinetics recorded over couple of minutes (Figure 2, 150 to 400 seconds). This longer time is needed for the dithionite to reach the molecules of NBD lipid-analog located initially in the inner part of the lipid bilayer. There are two possible scenarios to consider. First, the dithionite molecules might permeate through the membrane and quench the NBD lipid-analog inside of the vesicles. Second, the molecules of NBD lipid-analog located in the inner lipid layer of the vesicle can translocate (*i.e.* flop) to the outer lipid layer already exposed to the dithionite solution. The two scenarios are not mutually exclusive and can happen simultaneously.

A closer look at the quenching curves presented in Figure 2 reveals that the normalized fluorescence intensity drops initially to only ~0.65 instead of 0.5 as might have expected. This discrepancy between the results and the theory presented above is due to the fact that even after long extrusion through 100 nm pore polycarbonate membranes a small population of the vesicles is still expected to be multilamellar. The small vesicles encapsulated in larger ones are initially completely inaccessible to dithionite, thus increasing the fraction of the unquenched NBD lipid-analog molecules. This initial quenching is within the experimental error and identical to all the samples regardless of the sterol presence. We mention in passing that other factors that can influence the level of initial drop of fluorescence intensity may be: a) different pressure applied during extrusion of liposomes resulting in modified population of LUVs; b) different exposure of the lipid headgroup probe to the quencher depending on the phase of bilayer; c) difference in surface area of the inner and outer leaflet of the bilayer resulting in unequal concentration of the probe in the leaflets. Nevertheless, the level of initial drop of

fluorescence intensity is not expected to influence the following kinetics of quenching that is the subject of our study.

When comparing the results obtained for different sterols at longer time scale, it is striking that the case of 27-OH-chol is very distinct. While the quenching kinetics in POPC, POPC/chol and POPC/7β-OH-chol liposomes is similar, in POPC/27-OH-chol it is strongly accelerated. The speed of quenching calculated using Eq. 1 for all studied lipid composition follows the trend: POPC/chol $\lesssim$ POPC/7β-OH-chol $\lesssim$ POPC $\ll$ POPC/27-OH-chol. According to the two scenarios proposed earlier in the text, this result means that 27-OH-chol 1) increases the permeability of the lipid bilayer to dithionite and/or 2) increases the rate of NBD lipid flip-flop. While interrelated to each other, these two mechanisms imply modification of two distinct membrane characteristics that would have different consequences for biological membranes. Increased permeability reduces the asymmetry in the composition of the aqueous media separated by a membrane. Increased flip-flop rate, on the other hand, reduces asymmetry in lipid composition between the two layers of the bilayer. Both these asymmetries are abundant in living cells and both are vital for their functions. Distinguishing between the two scenarios is not an easy task. A number of experimental and computational data described below were collected in order to elucidate the molecular mechanism of membrane properties alterations induced by 27-OH-chol.

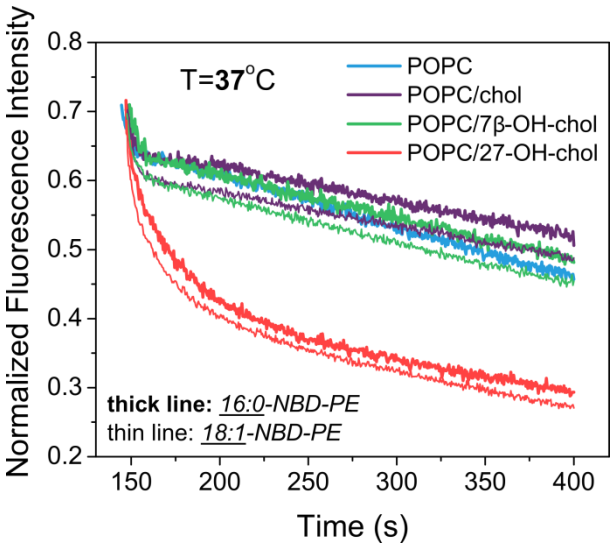

Figure 2. Fluorescence quenching kinetics of 16:0-NBD-PE (thick lines) and 18:1-NBD-PE (thin lines) embedded in liposomal membrane of 100 nm unilamellar vesicles by dithionite. Liposome bilayer compositions: POPC (blue); POPC with 10 mol% of cholesterol (purple); POPC with 10 mol% of 7β-OH-chol (green); POPC with 10 mol% of 27-OH-chol (red). Samples were measured at 37 °C.

Interestingly, the above-described results were very similar for two different NBD lipid-analogs. 18:1-NBD-PE has two unsaturated oleoyl chains in the place of saturated palmitoyl chains of 16:0-NBD-PE (see Figure 1). Based on these structural differences, one could expect that the two NBD lipids would differ in their flip-flop kinetics. At the same time the permeability of the membrane should be only marginally affected, since the fluorescent lipid content in the bilayer was only 0.5 mol%. In this view, the similarity of the 16:0-NBD-PE and 18:1-NBD-PE results (Figure 2, thick and thin lines, respectively) suggests that the rapid quenching induced by 27-OH-chol arises from increased membrane permeability to dithionite. Due to complexity of the studied processes, this finding is only a suggestive hint, not a proof.

To further examine the potential of 27-OH-chol to affect membrane properties, the dithionite quenching experiment was repeated for 16:0-NBD-PE embedded in DPPC liposomes. In contrast to POPC, both acyl chains of DPPC are fully saturated (Figure 1). At 27 °C (*i.e.*, below the main phase transition temperature of 41 °C), a DPPC bilayer is in the gel phase, where the diffusion of lipid molecules is strongly hindered. Under these circumstances, no flip-flop of phospholipids and a very low (if any) permeability of dithionite through the bilayer are expected. Indeed, as can be seen in Figure 3 (left panel), a very fast drop in fluorescence intensity after addition of dithionite to the sample is followed by an almost constant signal in the time range of 150-400 s. This behavior is observed consistently in all lipid compositions. However, at longer times, the kinetics recorded for DPPC/27-OH-chol/16:0-NBD-PE is noticeably faster than in the other systems (Figure 3, right panel). To quantify these results, the speed of quenching was evaluated using Eq. 1. As depicted in the inset in the right panel of Figure 3, the speed of quenching calculated for the DPPC/27-OH-chol/16:0-NBD-PE composition is significantly larger than for the other three systems.

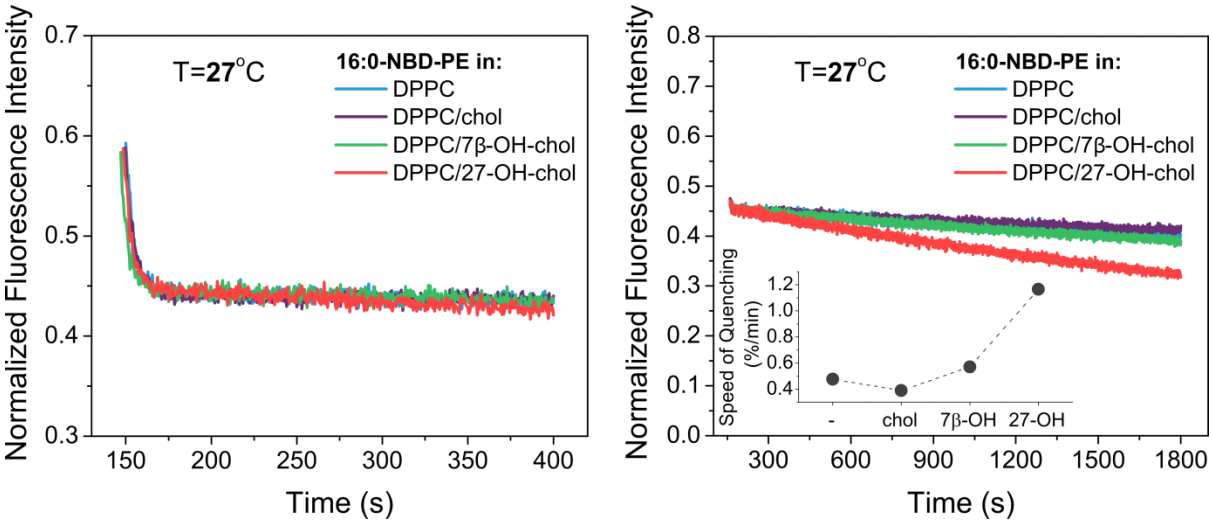

Figure 3. Short-time (left panel) and long-time (right panel) fluorescence quenching kinetics of 16:0-NBD-PE by dithionite. Liposome bilayer compositions were: DPPC (blue); DPPC with 10 mol% cholesterol (purple); DPPC with 10 mol% 7β-OH-chol (green); and DPPC with 10 mol% 27-OH-chol (red). Samples were measured at 27 °C. Right panel (inset): speed of quenching calculated using Eq. 1.

When the same DPPC-based samples were measured at 50 °C in their liquid-crystalline phase, the result (Figure 4) displayed the same trend for the speed of quenching as for POPC systems at 37 °C (Figure 2). The differences observed between the sterols in DPPC bilayers were slightly more pronounced than in POPC bilayers. The results for speed of quenching in POPC-based liposomes measured at 37 and DPPC-based systems at 50 °C are depicted in Figure 5, demonstrating again the exceptionally large quenching speed induced by 27-OH-chol.

Altogether, the results of the quenching experiments suggest that, unlike the other sterols, 27-OH-chol increases the permeability of lipid bilayers to a significant extent, while its influence on the rate of lipid flip-flops is unknown. Next, all-atom MD simulations were used to elucidate this issue in greater detail.

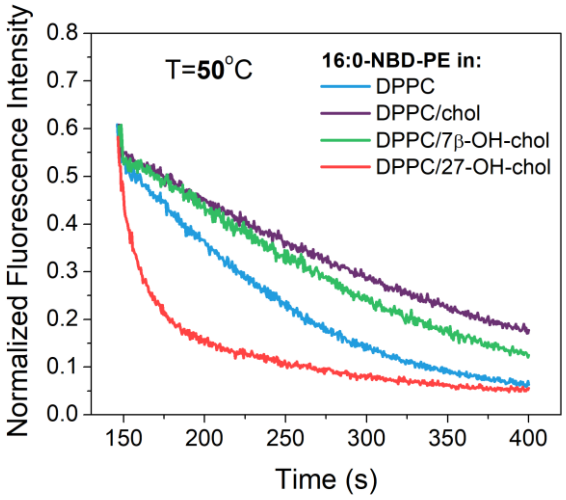

Figure 4. Fluorescence quenching kinetics of 16:0-NBD-PE by dithionite. Liposome bilayer compositions were: DPPC (blue); DPPC with 10 mol% cholesterol (purple); DPPC with 10 mol% 7β-OH-chol (green); and DPPC with 10 mol% 27-OH-chol (red). Samples were measured at 50 °C.

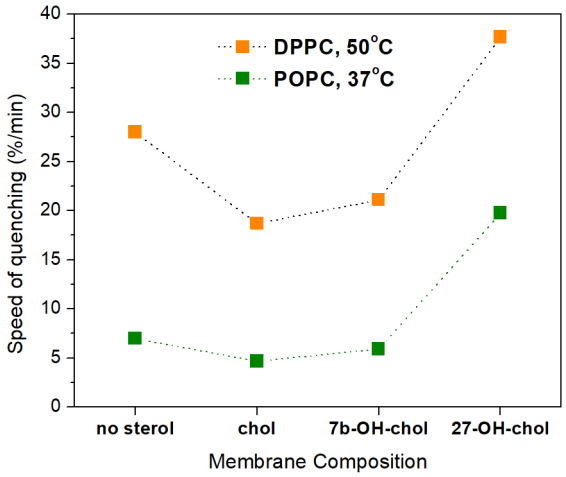

Figure 5. Speed of quenching, calculated according to Eq. 1. Liposomal bilayer composed of DPPC with/without 10 mol% sterol measured at 50 °C (orange); liposomal bilayer composed of POPC with/without 10 mol% sterol measured at 37 °C (green). 16:0-NBD-PE fluorescence probe incorporated in bilayer was quenched by dithionite.

Free Energy Profiles Exclude Lipid Flip-Flop as a Fluorescence Quenching Mechanism

Figure 6 shows the free energy profiles of a single POPC molecule carrying out a flip-flop from one leaflet to the other in bilayers composed of pure POPC (blue), POPC with 10 mol% cholesterol (purple), POPC with 10 mol% 7β-OH-chol (green), and POPC with 10 mol% 27-OH-chol (red). In all cases the free energy profile shows a minimum around z = 2 nm and z = −2 nm (*i.e.*, corresponding to the equilibrium positions of POPC in a lipid bilayer) and a maximum at z = 0 nm (*i.e.*, for the POPC headgroup located in the middle of the lipid bilayer). Also, as expected, the free energy increases at $z > 3$ nm and $z < -3$ nm (*i.e.*, when POPCs move from the bilayer to the water phase). The free energy barriers for the flip-flop of POPC in the sterol-containing and pure POPC bilayers are ~90 and ~50 kJ/mol, respectively. These high values provide compelling evidence that changes in flip-flop rates cannot be the explanation for the observed differences in fluorescence quenching speeds discussed above. Based on these free energy results, spontaneous lipid flip-flops across a bilayer are extremely slow: typical flip-flop rates with similar free energy barriers are in the ballpark of 10^{-15} s^{-1}, corresponding to rates where on average a single lipid would flip-flop once every 24 h [55-56], and sterols that rigidify membranes will further slow these processes down. While in our simulations we did not consider the translocation of fluorescent lipids (such as 18:1-NBD-PE), this conclusion applies to them, too, since the NBD unit increases probe's polarity in the head group region and is, therefore, expected to increase the translocation barrier from one leaflet to the other. Figure 6 also highlights an essential feature between the three sterol-containing systems: the

free energy barriers of POPC/chol, POPC/7β-OH-chol and POPC/27-OH-chol for flip-flop are largely similar, *i.e.*, of the order of 80-90 kJ/mol, being much larger than the barrier of the POPC system, strongly supporting the view that flip-flops are extremely rare.

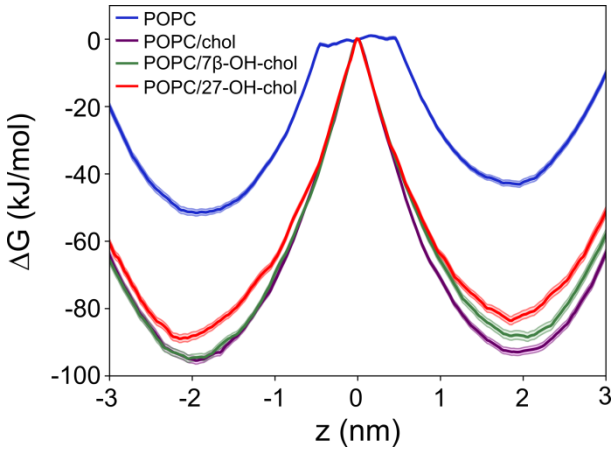

Figure 6. Free energy profiles for a single POPC molecule passing through a lipid bilayer. POPC molecule was pulled through a bilayer composed of pure POPC (blue); POPC with 10 mol% cholesterol (purple); POPC with 10 mol% 7β-OH-chol (green); POPC with 10 mol% 27-OH-chol (red). The location z = 0 corresponds to the center of a lipid bilayer.

Free Energy Profiles of Water Translocations Support the Oxysterol-Driven Mechanism of Membrane Permeation

To estimate the effects of the three sterols on the permeability of a lipid bilayer, we used umbrella-sampling simulations to calculate the free energy barrier for a water molecule to pass through a lipid bilayer. Permeability can be studied in many ways; here the water molecule is used as representative of small and polar molecules passing through a lipid bilayer. Figure 7 depicts the free energy profiles in the four different systems studied. In all cases, the free energy profile has a shallow local minimum in the middle of the bilayer and a maximum at about 0.4 – 0.5 nm from the membrane center. Most important, however, is the free energy barrier that a water molecule has to overcome to pass through the bilayer. The barrier is the largest in POPC/chol, followed in decreasing order by POPC/7β-OH-chol, POPC, and POPC/27-OH-chol. Assuming that permeation is an activated process, the free energy data suggest that permeation of water and related small polar molecules would be the fastest in POPC/27-OH-chol, followed (in order of decreasing permeation rate) by POPC, POPC/7β-OH-chol, and POPC/chol, which is consistent with the results of fluorescence quenching experiments shown in Figures 2, 4, and 5.

Atomic-scale simulations together with fluorescence quenching experiments performed on LUVs are thus supporting the view that 27-OH-chol increases the permeability of POPC bilayer to polar molecules.

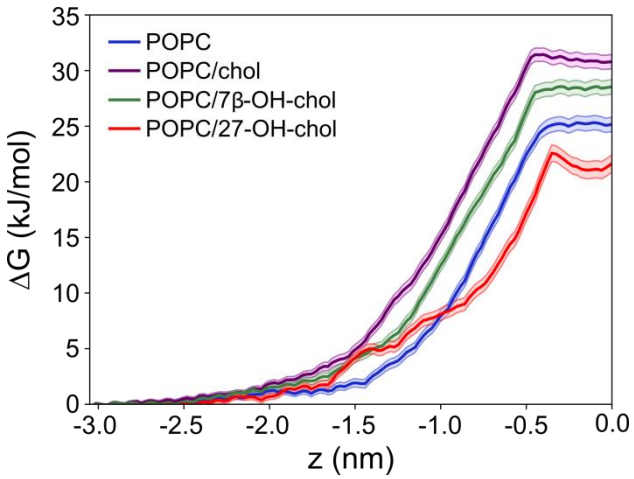

Figure 7. Free energy profiles for a single water molecule permeating through a lipid bilayer. Water molecule was pulled through a bilayer composed of pure POPC (blue); POPC with 10 mol% cholesterol (purple); POPC with 10 mol% 7β-OH-chol (green); POPC with 10 mol% 27-OH-chol (red). The position $z = 0$ corresponds to the center of the lipid bilayer. For clarity, only half of the lipid bilayer is shown.

Multivesicular Liposomes Serve as a Proof of Membrane Permeabilization by 27-OH-chol

The above collected evidence supports increased permeability of POPC/27-OH-chol membrane as a more probable source of the accelerated quenching kinetics in this system then the augmented flip-flop of lipids. In the search for the ultimate answer to this problem, we performed NBD-dithionite quenching experiments on giant vesicles with a fluorescence confocal microscope at various conditions. Interestingly, we found that giant liposomes that encapsulate other vesicles inside them provide a convincing proof for the increased membrane permeability scenario. Figure 8 presents such a liposome composed of POPC/27-OH-chol lipid mixture in a series of images collected at different times after addition of dithionite to the sample. This so-called multivesicular liposome consists of 3 distinct GUVs that are nested within one another like Russian dolls. The time evolution depicted in Figure 8 demonstrates that the fluorescent probes in the membranes of the three GUVs are quenched in a series, one after another, starting from the outermost membrane. Shortly after addition of dithionite to the sample, we observed that NBD lipid molecules in the outermost GUV membrane were quenched first (Figure 8, 5 min). The images at later times (10-25 minutes) show that the

fluorescence intensity measured from the membranes of inner GUVs decreases, one at a time, until all fluorescence is gone. Since the inner GUVs can be quenched only if dithionite permeates through outer GUVs, these results proof that 27-OH-chol does indeed facilitate the lipid bilayer permeability to dithionite.

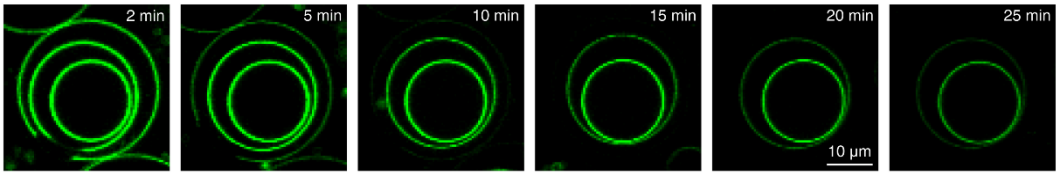

Figure 8. 18:1-NBD-PE incorporated into encapsulated POPC/27-OH-chol GUV membranes quenched by dithionite. The images (from left to right) highlight a sequence of pictures collected in time after addition of the quencher to the space outside the multivesicular liposome. Measurements were performed at 25 °C.

4. DISCUSSION

Similarly to cholesterol, also oxysterols affect the physical properties of lipid bilayers [39]. Ring-oxidized sterols: 7-ketocholesterol, 7α-hydroxycholesterol, 7β-OH-chol, 4β-hydroxycholesterol, 3β,5α,6β-trihydroxycholestane increase ordering of the acyl tails, increase membrane thickness, and decreased surface area per lipid; thus induce changes similar to cholesterol; however, cholesterol affects membrane properties stronger than ring-oxidized oxysterol. The observed difference between ring-oxidized sterol and cholesterol results from larger tilting of ring-oxidized oxysterols, which allows the hydration of all polar groups. The changes induced by ring-oxidized oxysterols suggest that also the permeability of the bilayer should be reduced. In our current studies, we indeed observed that 7β-OH-chol decreases membrane permeability (Figures 4 and 7), but the effect of cholesterol is stronger.

Tail-oxidized oxysterols: 27-hydroxycholesterol, 24S-hydroxycholesterol, 25-hydroxycholesterol, and 25S-cholestenoic acid also induce above mentioned changes of the lipid bilayer properties, and for some measured parameters they are equal to cholesterol; nevertheless, the behavior of tail-oxidized oxysterols is more complicated. In our previous studies, 27-OH-chol was found to move very fast back and forth between the two adjacent lipid leaflets, without changing its orientation [57]. We called this process “bobbing” to differentiate it from the standard flip-flop process, which involves reorientation of a molecule. Bobbing of tail-oxidized sterols is associated with local deformation of the bilayer structure: bilayer becomes thinner, allowing for temporal connection between water and –OH groups of 27-OH-chol at two opposite water–membrane interfaces. Such deformation may increase membrane

permeability. Moreover, in previous studies of 25-OH-chol it was suggested that this oxysterol could act as a "shuttle", promoting permeation of glucose and calcium [37].

Based on the results of fluorescence quenching experiments performed on liposomal dispersions in the present work, one can conclude that the tail-oxidized sterol (27-OH-chol) speeds up the quenching process significantly. Additional measurements and atomic-scale simulations helped us to identify and explore two possible mechanisms underlying this difference: 1) increased permeability of the lipid bilayer to the quencher (dithionite), and 2) increased flip-flop of the fluorescent lipid analog.

We found that the quenching kinetics of two different NBD lipid analogs was very similar, which suggests that the mechanism employed by 27-OH-chol is not likely based on increasing lipid flip-flop rate. This hypothesis is supported by our biomolecular simulation results, showing that the free energy barriers calculated for phospholipid translocation events contradict the idea that 27-OH-chol would foster lipid flip-flop more than 7β-OH-chol or cholesterol. Importantly, the free energy calculations also showed that 27-OH-chol enhances permeation of water molecules through a POPC bilayer: the free energy barrier of water permeation (Figure 7) is the smallest in bilayers comprised of 27-OH-chol and POPC, and the trend among the different studied systems (Figure 7) is consistent with that observed in the fluorescence quenching data.

Altogether, we found that the studied oxysterols do not seem to influence lipid flip-flop kinetics differently to any significant degree than cholesterol. We did find, however, that 27-OH-chol permeabilizes a POPC bilayer to dithionite and water. This behavior is in accord with previous studies, which showed that 25-OH-chol (another member in the family of tail-oxidized oxysterols) increases membrane permeability for calcium and glucose [12, 36, 58].

5. CONCLUSIONS

We demonstrate that 27-OH-chol as a tail-oxidized sterol promotes membrane permeability to dithionite (anionic molecule) and water (polar molecule)., Putting this together with older studies showing increases of membrane permeability for calcium (cation) and glucose (hydrophilic molecule) due to the presence of 25-OH-chol, we can thus conclude that tail-oxidized sterols promote permeation of small charged and hydrophilic molecules and water. Our atomic-scale biomolecular simulations strongly suggest bobbing [57] and related deformation of bilayer structure as a generic mechanism for tail-oxidized sterols facilitating permeability. In contrast, ring-oxidized sterols do not compromise permeability of lipid bilayers. These differences exemplify the distinct roles of the two classes of oxysterols.

ACKNOWLEDGEMENTS

We thank the Academy of Finland for financial support: the Finland Distinguished Professor (FiDiPro, Grant no. 263410) program (W.K.) and the Center of Excellence (W.K., H.M., T.R., I.V.) funding (Grant no. 272130)). I.V. thanks the European Research Council (Advanced Grant CROWDED-PRO-LIPIDS), Sigrid Juselius Foundation, and the Helsinki Institute of Life Science (HiLIFE) Fellow program. P.Jur., P.Jun., and M.H. thank the Czech Science Foundation for support via an EXPRO grant no. 19-26854X. T.Cz. acknowledges the Erasmus project. L.C. acknowledges the support from NF Neuron and the Czech Science Foundation (grant 18-26751S). A.O. acknowledges the Czech Science Foundation (grant 17-06792S). CSC—IT Centre for Science (Espoo, Finland) is acknowledged for computational resources (project number tty3995). We also acknowledge computer resources granted by the Finnish Grid and Cloud Infrastructure (persistent identifier urn:nbn:fi:research-infras-2016072533).

REFERENCES

1. Finkelstein, A.; Cass, A., Effect of cholesterol on water permeability of thin lipid membranes. *Nature* **1967,** *216* (5116), 717-718.
2. Mathai, J. C.; Tristram-Nagle, S.; Nagle, J. F.; Zeidel, M. L., Structural determinants of water permeability through the lipid membrane. *The Journal of General Physiology* **2008,** *131* (1), 69-76.
3. Subczynski, W. K.; Wisniewska, A.; Yin, J. J.; Hyde, J. S.; Kusumi, A., Hydrophobic barriers of lipid bilayer - Membranes formed by reduction of water penetration by alkyl chain unsaturation and cholesterol. *Biochemistry* **1994,** *33* (24), 7670-7681.
4. Marsh, D., Polarity and permeation profiles in lipid membranes. *Proceedings of the National Academy of Sciences of the United States of America* **2001,** *98* (14), 7777-7782.
5. Shinoda, W., Permeability across lipid membranes. *Biochimica et Biophysica Acta (BBA)-Biomembranes* **2016,** *1858* (10), 2254-2265.
6. Saito, Y.; Yoshida, Y.; Niki, E., Cholesterol is more susceptible to oxidation than linoleates in cultured cells under oxidative stress induced by selenium deficiency and free radicals. *FEBS Letters* **2007,** *581* (22), 4349-4354.
7. Hong, C.; Tieleman, D. P.; Wang, Y., Microsecond Molecular Dynamics Simulations of Lipid Mixing. *Langmuir* **2014,** *30* (40), 11993-12001.
8. Haines, T. H., Water transport across biological membranes. *FEBS Letters* **1994,** *346* (1), 115-122.
9. Waldeck, A. R.; Nouri-Sorkhabi, M. H.; Sullivan, D. R.; Kuchel, P. W., Effects of cholesterol on transmembrane water diffusion in human erythrocytes measured using pulsed field gradient NMR. *Biophysical Chemistry* **1995,** *55* (3), 197-208.
10. Kitson, N.; Thewalt, J.; Lafleur, M.; Bloom, M., A Model Membrane Approach to the Epidermal Permeability Barrier. *Biochemistry* **1994,** *33* (21), 6707-6715.

11. Papahadjopoulos, D.; Nir, S.; Ohki, S., Permeability properties of phospholipid membranes - Effect of cholesterol and temperature. *Biochim. Biophys. Acta* **1972,** *266* (3), 561-583.
12. Demel, R. A.; Bruckdorfer, K. R.; Vandeene.Ll, Effect of sterol structure on permeability of liposomes to glucose, glycerol and Rb+. *Biochim. Biophys. Acta* **1972,** *255* (1), 321-330.
13. Ranadive, G. N.; Lala, A. K., Sterol-phospholipid interaction in model membranes - Role of C5-C6 double-bond in cholesterol. *Biochemistry* **1987,** *26* (9), 2426-2431.
14. Subczynski, W. K.; Hyde, J. S.; Kusumi, A., Effect if alkyl chain unsaturation and cholesterol intercalation on oxygen-transport in membranes - A pulse ESR spin labeling study. *Biochemistry* **1991,** *30* (35), 8578-8590.
15. Shea, R.; Smith, C.; Pias, S. C., Chapter 6: Magnification of Cholesterol-Induced Membrane Resistance on the Tissue Level: Implications for Hypoxia. *Advances in Experimental Medicine and Biology* **2016,** *923*, 43-50.
16. Khajeh, A.; Modarress, H., The influence of cholesterol on interactions and dynamics of ibuprofen in a lipid bilayer. *Biochimica et Biophysica Acta (BBA)-Biomembranes* **2014,** *1838* (10), 2431-2438.
17. Khajeh, A.; Modarress, H., Effect of cholesterol on behavior of 5-fluorouracil (5-FU) in a DMPC lipid bilayer, a molecular dynamics study. *Biophysical Chemistry* **2014,** *187*, 43-50.
18. Sun, D.; Lin, X.; Gu, N., Cholesterol affects C 60 translocation across lipid bilayers. *Soft Matter* **2014,** *10* (13), 2160-2168.
19. Deng, D.; Jiang, N.; Hao, S.-J.; Sun, H.; Zhang, G.-j., Loss of membrane cholesterol influences lysosomal permeability to potassium ions and protons. *Biochimica et Biophysica Acta (BBA)-Biomembranes* **2009,** *1788* (2), 470-476.
20. Ohvo-Rekila, H.; Ramstedt, B.; Leppimaki, P.; Slotte, J. P., Cholesterol interactions with phospholipids in membranes. *Progress in Lipid Research* **2002,** *41* (1), 66-97.
21. Róg, T.; Vattulainen, I., Cholesterol, sphingolipids, and glycolipids: What do we know about their role in raft-like membranes? *Chemistry and Physics of Lipids* **2014,** *184* (0), 82-104.
22. Venable, R. M.; Krämer, A.; Pastor, R. W., Molecular Dynamics Simulations of Membrane Permeability. *Chemical reviews* **2019,** *119* (9), 5954-5997.
23. Paula, S.; Volkov, A.; Van Hoek, A.; Haines, T.; Deamer, D. W., Permeation of protons, potassium ions, and small polar molecules through phospholipid bilayers as a function of membrane thickness. *Biophysical Journal* **1996,** *70* (1), 339-348.
24. Xiang, T.-X.; Anderson, B. D., Phospholipid surface density determines the partitioning and permeability of acetic acid in DMPC: cholesterol bilayers. *Journal of Membrane Biology* **1995,** *148* (2), 157-167.
25. van Meer, G.; Voelker, D. R.; Feigenson, G. W., Membrane lipids: where they are and how they behave. *Nature Reviews Molecular Cell Biology* **2008,** *9* (2), 112-124.
26. Wertz, P. W.; van den Bergh, B., The physical, chemical and functional properties of lipids in the skin and other biological barriers. *Chemistry and Physics of Lipids* **1998,** *91* (2), 85-96.
27. Kitson, N.; Monck, M.; Wong, K.; Thewalt, J.; Cullis, P., The influence of cholesterol 3-sulphate on phase behaviour and hydrocarbon order in model membrane systems. *Biochimica et Biophysica Acta (BBA)-Biomembranes* **1992,** *1111* (1), 127-133.
28. Zhang, J.; Liu, Q., Cholesterol metabolism and homeostasis in the brain. *Protein & Cell* **2015,** *6* (4), 254-264.
29. Bunker, A.; Magarkar, A.; Viitala, T., Rational design of liposomal drug delivery systems, a review: Combined experimental and computational studies of lipid membranes, liposomes and their PEGylation. *Biochimica et Biophysica Acta (BBA)-Biomembranes* **2016,** *1858* (10), 2334-2352.

30. Dhawan, V.; Magarkar, A.; Joshi, G.; Makhija, D.; Jain, A.; Shah, J.; Reddy, B.; Krishnapriya, M.; Róg, T.; Bunker, A., Stearylated cycloarginine nanosystems for intracellular delivery–simulations, formulation and proof of concept. *RSC Advances* **2016,** *6* (114), 113538-113550.
31. Pathak, P.; Dhawan, V.; Magarkar, A.; Danne, R.; Govindarajan, S.; Ghosh, S.; Steiniger, F.; Chaudhari, P.; Gopal, V.; Bunker, A., Design of cholesterol arabinogalactan anchored liposomes for asialoglycoprotein receptor mediated targeting to hepatocellular carcinoma: In silico modeling, in vitro and in vivo evaluation. *International Journal of Pharmaceutics* **2016,** *509* (1), 149-158.
32. Mayer, L. D.; Bally, M. B.; Cullis, P. R., Strategies for optimizing liposomal doxorubicin. *Journal of Liposome Research* **1990,** *1* (4), 463-480.
33. Barenholz, Y. C., Doxil®—the first FDA-approved nano-drug: lessons learned. *Journal of Controlled Release* **2012,** *160* (2), 117-134.
34. Gill, S.; Chow, R.; Brown, A. J., Sterol regulators of cholesterol homeostasis and beyond: The oxysterol hypothesis revisited and revised. *Progress in Lipid Research* **2008,** *47* (6), 391-404.
35. Kulig, W.; Cwiklik, L.; Jurkiewicz, P.; Rog, T.; Vattulainen, I., Cholesterol oxidation products and their biological importance. *Chemistry and Physics of Lipids* **2016,** *199*, 144-160.
36. Boissonneault, G. A.; Heiniger, H.-J., 25-Hydroxycholesterol-induced elevations in 45Ca uptake: Permeability changes in P815 cells. *Journal of Cellular Physiology* **1985,** *125* (3), 471-475.
37. Theunissen, J. J. H.; Jackson, R. L.; Kempen, H. J. M.; Demel, R. A., Membrane properties of oxysterols. Interfacial orientation, influence on membrane permeability and redistribution between membranes. *Biochimica et Biophysica Acta (BBA) - Biomembranes* **1986,** *860* (1), 66-74.
38. Parra-Ortiz, E.; Browning, K. L.; Damgaard, L. S. E.; Nordström, R.; Micciulla, S.; Bucciarelli, S.; Malmsten, M., Effects of oxidation on the physicochemical properties of polyunsaturated lipid membranes. *Journal of Colloid and Interface Science* **2019,** *538*, 404-419.
39. Kulig, W.; Olżyńska, A.; Jurkiewicz, P.; Kantola, A. M.; Komulainen, S.; Manna, M.; Pourmousa, M.; Vazdar, M.; Cwiklik, L.; Rog, T.; Khelashvili, G.; Harries, D.; Telkki, V.-V.; Hof, M.; Vattulainen, I.; Jungwirth, P., Cholesterol under oxidative stress—How lipid membranes sense oxidation as cholesterol is being replaced by oxysterols. *Free Radical Biology and Medicine* **2015,** *84*, 30-41.
40. Enkavi, G.; Javanainen, M.; Kulig, W.; Róg, T.; Vattulainen, I., Multiscale Simulations of Biological Membranes: The Challenge To Understand Biological Phenomena in a Living Substance. *Chemical Reviews* **2019,** *119* (9), 5607-5774.
41. Angelova, M.; Soléau, S.; Méléard, P.; Faucon, F.; Bothorel, P., Preparation of giant vesicles by external AC electric fields. Kinetics and applications. In *Trends in Colloid and Interface Science VI*, Springer: 1992; pp 127-131.
42. Koukalová, A.; Pokorná, Š.; Fišer, R.; Kopecký, V.; Humpolíčková, J.; Černý, J.; Hof, M., Membrane activity of the pentaene macrolide didehydroroflamycoin in model lipid bilayers. *Biochimica et Biophysica Acta (BBA)-Biomembranes* **2015,** *1848* (2), 444-452.
43. Jorgensen, W. L.; Maxwell, D. S.; TiradoRives, J., Development and testing of the OPLS all-atom force field on conformational energetics and properties of organic liquids. *Journal of the American Chemical Society* **1996,** *118* (45), 11225-11236.
44. Kaminski, G. A.; Friesner, R. A.; Tirado-Rives, J.; Jorgensen, W. L., Evaluation and reparametrization of the OPLS-AA force field for proteins via comparison with accurate quantum chemical calculations on peptides. *Journal of Physical Chemistry B* **2001,** *105* (28), 6474-6487.

45. Maciejewski, A.; Pasenkiewicz-Gierula, M.; Cramariuc, O.; Vattulainen, I.; Rog, T., Refined OPLS All-Atom Force Field for Saturated Phosphatidylcholine Bilayers at Full Hydration. *Journal of Physical Chemistry B* **2014,** *118* (17), 4571-4581.
46. Kulig, W.; Pasenkiewicz-Gierula, M.; Róg, T., Topologies, structures and parameter files for lipid simulations in GROMACS with the OPLS-aa force field: DPPC, POPC, DOPC, PEPC, and cholesterol. *Data in Brief* **2015,** *5*, 333-336.
47. Hess, B.; Bekker, H.; Berendsen, H. J. C.; Fraaije, J., LINCS: A linear constraint solver for molecular simulations. *Journal of Computational Chemistry* **1997,** *18* (12), 1463-1472.
48. Miyamoto, S.; Kollman, P. A., SETTLE - An Analytical Version of the SHAKE and RATTLE Algorithm for Rigid Water Models. *Journal of Computational Chemistry* **1992,** *13* (8), 952-962.
49. Essmann, U.; Perera, L.; Berkowitz, M. L.; Darden, T.; Lee, H.; Pedersen, L. G., A Smooth Particle Mesh Ewald Method. *Journal of Chemical Physics* **1995,** *103* (19), 8577-8593.
50. Nose, S., A Molecular-Dynamics Method for Simulations in the Canonical Ensemble. *Molecular Physics* **1984,** *52* (2), 255-268.
51. Hoover, W. G., Canonical Dynamics - Equilibrium Phase-Space Distribution. *Physical Review A* **1985,** *31* (3), 1695-1697.
52. Parrinello, M.; Rahman, A., Polymorphic Transitions in Single-Crystals - A New Molecular-Dynamics Method. *Journal of Applied Physics* **1981,** *52* (12), 7182-7190.
53. Berendsen, H. J.; van der Spoel, D.; van Drunen, R., GROMACS: a message-passing parallel molecular dynamics implementation. *Computer Physics Communications* **1995,** *91* (1-3), 43-56.
54. Hess, B.; Kutzner, C.; van der Spoel, D.; Lindahl, E., GROMACS 4: Algorithms for highly efficient, load-balanced, and scalable molecular simulation. *Journal of Chemical Theory and Computation* **2008,** *4* (3), 435-447.
55. Nakano, M.; Fukuda, M.; Kudo, T.; Matsuzaki, N.; Azuma, T.; Sekine, K.; Endo, H.; Handa, T., Flip-flop of phospholipids in vesicles: kinetic analysis with time-resolved small-angle neutron scattering. *The Journal of Physical Chemistry B* **2009,** *113* (19), 6745-6748.
56. McConnell, H. M.; Kornberg, R. D., Inside-outside transitions of phospholipids in vesicle membranes. *Biochemistry* **1971,** *10* (7), 1111-1120.
57. Kulig, W.; Mikkolainen, H.; Olżyńska, A.; Jurkiewicz, P.; Cwiklik, L.; Hof, M.; Vattulainen, I.; Jungwirth, P.; Rog, T., Bobbing of Oxysterols: Molecular Mechanism for Translocation of Tail-Oxidized Sterols through Biological Membranes. *The Journal of Physical Chemistry Letters* **2018,** *9* (5), 1118-1123.
58. Holmes, R. P.; Yoss, N. L., 25-Hydroxysterols increase the permeability of liposomes to Ca2+ and other cations. *Biochimica et Biophysica Acta (BBA) - Biomembranes* **1984,** *770* (1), 15-21.

Table of Contents Graphic